Hindawi
International Transactions on Electrical Energy Systems
Volume 2023, Article ID 7990690, 18 pages
https://doi.org/10.1155/2023/7990690

Research Article

Battery Cell Balancing of V2G-Equipped Microgrid in the Presence of Energy Storage Aggregator

Geno Peter,[1] **Albert Alexander Stonier**,[2] **Dishore Shunmugham Vanaja**,[3] **Fitrahsya Justin**,[4] **Ramya Kuppusamy**,[5] **and Yuvaraja Teekaraman**[6]

[1]*CRISD, School of Engineering and Technology, University of Technology Sarawak, Sibu, Malaysia*
[2]*School of Electrical Engineering, Vellore Institute of Technology, Vellore, Tamil Nadu, India*
[3]*Electrical Engineering Department, Mar Baselios College of Engineering and Technology, Thiruvananthapuram, Kerala, India*
[4]*Balingian Power Generation Sdn. Bhd, Sarawak Energy Berhad, Kuching, Malaysia*
[5]*Department of Electrical and Electronics Engineering, Sri Sairam College of Engineering, Bangalore 562 106, India*
[6]*School of Engineering & Computing, American International University, Al Jahra, Kuwait*

Correspondence should be addressed to Yuvaraja Teekaraman; yuvarajastr@ieee.org

Received 21 May 2023; Revised 26 September 2023; Accepted 24 October 2023; Published 9 November 2023

Academic Editor: N. Prabaharan

High electricity consumption in Sarawak's cities is a concern, driven by residential, industrial, and commercial users. Greater demand for electrical energy requires more electrical resources, affecting grid stability. To prevent blackouts and enhance grid resilience, electric vehicles can serve as distributed energy storage in microgrids. The biggest problem facing energy storage is that not all batteries within energy storage are the same. Every battery cell in the battery pack has a different rate of self-discharge, capacity, internal resistance, and aging, even though they have the same chemical and physical characteristics. These variations lead to power imbalances in energy storage. Therefore, to address this issue, a unique voltage equalization method using a modular flyback converter is presented. Its core objective is to correct voltage imbalances among batteries. The proposed method is modelled using MATLAB, and the performance of the system has been evaluated. Furthermore, the developed model is implemented in a microgrid and tested for two different cases (with and without energy storage for electric cars). From the simulation outcomes, it has been verified that the developed cell balancing technique performs well in equalizing the voltage of cells than the conventional methods.

1. Introduction

High electricity usage and load demand in Sarawak cities are caused by consumers from various backgrounds, including residential, commercial, and industrial consumers. As a result, renewable energy sources are becoming increasingly popular because they can meet the demand for electrical energy while also resolving the problem of electrical energy deficit. The use of renewable energy sources consists of a variety of configurations in the electricity generation system. One of the most common configurations is the use of photovoltaic solar generation in the microgrid system [1]. Photovoltaic resources are more desirable for microgrid use because they do not have any moving components and there are no losses associated with motion. But its intermittent nature is the main drawback of solar power. Hence, energy storage systems [2] are generally recommended for intermittent sources. The increasing penetration of the PV system may also have significant effects on power distribution systems soon, especially because of the intermittent nature of its output caused by cloud cover. Coordinated use of the solar power system with electric vehicles will therefore be a possible solution that can help maintain the grid's flat power profile [3]. Since electric vehicles are parked on average 22 hours a day at work or home, the microgrid can integrate electric vehicles as an energy storage unit. When parked and plugged into the electrical grid, electric vehicles can consume and store energy and will also be able to supply

power back to the grid when needed [4]. Electric vehicles which are used as energy storage for microgrid consist of a larger battery pack and an electric motor. The battery pack is a combination of cells connected in series and parallel to obtain the desired operating voltage and current rating. The batteries of electric vehicles are developed by stacking many individual cells in a specific order. According to [5], the electric vehicle batteries are not similar to those used in electronic devices. Electric vehicle batteries needed to withstand high energy and power capacity within several limits in terms of space and weight. Lithium-ion cells are recommended storage technologies for EVs due to their high energy capacity, affordable price, longer lifespan, and also low self-discharge rate. However, due to the dynamic behaviour of charging and discharging of EVs, the capacity of the battery pack is not constant, leading to a power imbalance. Balancing plays a crucial role in preserving battery life [6] because, without it, cell voltages can gradually deviate over time. This divergence in voltage levels can lead to a rapid decline in the overall capacity of the battery pack during its use, ultimately jeopardizing the integrity of the entire battery system and diminishing its lifespan. This issue becomes particularly critical in high-voltage battery systems, such as those commonly used in hybrid electric vehicles (hybrid EVs) [7, 8] that rely on regenerative braking. Hence, it becomes imperative for the battery management system (BMS) to incorporate an efficient balancing mechanism.

In an electric vehicle battery pack, individual cell voltages tend to diverge over time due to variations in state of charge (SOC), impedance, capacity, self-discharge rate, and temperature characteristics. Cell balancing serves the dual purpose of extending battery lifespan and enhancing safety. The passive balancing technique [9] is a simple and easily implementable method which makes the overcharged cell dissipate excess energy using a bypass technique. This approach provides a cost-effective solution for cell balancing and is commonly used in industrial applications. On the other hand, active balancing employs capacitive or inductive methods to efficiently transfer charge from overcharged to undercharged cells. A fixed-shunting resistor-based passive balancing method is introduced in [10]. The authors have implemented a method for balancing the cells of the lithium battery. The limitation of this method is heat dissipation, and it can be used for only less number of cells connected in series. The authors in [11] developed a switched shunting resistor-based passive balancing method. This method can be used only for low-voltage applications, and it affects the battery life. A cell bypass active balancing method is introduced in [12]. The method is very cheap and very easy to control. The switches used in the cell bypass method experience high current stress, which increases the losses in the system. The authors in [13] developed a cell-to-cell active balancing method for high-power applications. However, this method makes the system bulky and is very difficult to control. The cell-to-pack active balancing method is introduced in [14]. This topology suffers from higher voltage and current stress as well as being very expensive. The pack-to-cell active balancing method is introduced in [15]. In this topology, the maintenance can be more challenging due to the need to access and service individual cells within the pack. The cell to pack-to-cell topology is implemented in [16]. It allows for a more efficient use of cell space, potentially reducing the overall weight and size of the battery pack. It simplifies battery management as cells are grouped, but can still require robust balancing and monitoring.

Cybersecurity concerns in EV charging stations [17] arise from the extensive data exchange between the charging infrastructure, vehicles, and user accounts. This data includes personal information, billing details, and vehicle-related data, making it a prime target for cybercriminals. Malware and ransomware attacks can compromise the software running in EV charging stations. An attack can disrupt service, potentially leaving EV drivers stranded, and attackers may demand ransoms for restoring functionality.

From the literature, the key research gaps identified in the balancing systems are as follows:

(i) Passive balancing wastes excess energy as heat during balancing, reducing overall efficiency

(ii) Passive balancing process potentially requiring additional cooling measures

(iii) Passive balancing process is a slower balancing process as it relies on the natural discharge of overcharged cells

(iv) Active balancing is more energy-efficient as it transfers charge instead of dissipating it, but some energy loss still occurs

(v) Active balancing requires additional components such as capacitors or inductors, increasing system complexity and cost

(vi) Active balancing systems may have more points of potential failure due to additional components.

From the research gaps, the objectives of the proposed system are framed.

(i) To choose a suitable approach for battery modelling in order to anticipate charge/discharge behaviours, state of charge, voltage, and various battery attributes

(ii) To design a two-switch flyback converter by considering the drawbacks of a conventional flyback converter

(iii) To implement a modified balancing method which overcomes the drawbacks of the existing methods

(iv) To test the developed balancing method in a microgrid system with a battery aggregator

(v) To compare the effectiveness of the suggested technique with the existing methods

The work mainly concentrates on two approaches. The first approach is to integrate electric cars as one energy storage aggregator and model the aggregator for the microgrid. The second approach is to implement the developed battery balancing method to balance the voltage of the total battery packs inside electric vehicles. This is because if there is a difference between the voltage and the capacity of

the attached battery cells, the entire battery pack cannot function efficiently, which has led to an energy storage imbalance [18]. The energy storage capacity is reduced and cannot work efficiently when connected to the microgrid. The paper is organized as follows: Section 2 discusses the modelling of the battery. Section 3 discusses the proposed converter design. Section 4 discusses the developed balancing method. Section 5 presents the results of the entire system. Section 6 presents the conclusion of the developed system, pointing out the highlights of the proposed balancing method.

2. Battery Modelling

In order to create a battery-powered system that functions effectively, a precise battery model becomes imperative. Such a model possesses the capability to anticipate both the dynamic and steady-state behaviours of the battery. In practice, crafting a precise model for different battery chemistries poses a significant challenge, primarily because of the intricate electrochemical nature of batteries. Depending on the trade-off between system accuracy and implementation complexity, the extended Thevenin model [19] can effectively capture battery transients at various levels, ranging from 1RC to 2RC and 3RC, up to the nth order model. Consequently, the implementation of RC models is adopted to enhance the performance of EVs battery management systems (BMS).

2.1. 3RC Battery Model. The framework for solving the optimal cell balancing problem is based on the Thevenin 3RC electrical equivalent circuit model (ECM). Electrochemical impedance spectroscopy (EIS) is a test used to derive model parameters. Figure 1 illustrates the ECM featuring three parallel RC pairs.

$$V_t = V_{\text{oc}} - R_0 i - V_{R1C1} - V_{R2C2} - V_{R3C3}, \tag{1}$$

where, V_{R1C1},V_{R2C2},V_{R3C3} are the voltages of the shunt RC pair, represents the output voltage of the 3RC model, equation (2) represents the transient voltage response of the system.

$$\left.\begin{aligned} \frac{\mathrm{d}V_{R_1C_1}}{\mathrm{dt}} &= \frac{i}{C1} - \frac{V_{R_1C_1}}{R_1C_1} \\ \frac{\mathrm{d}V_{R_2C_2}}{\mathrm{dt}} &= \frac{i}{C2} - \frac{V_{R_2C_2}}{R_2C_2} \\ \frac{\mathrm{d}V_{R_3C_3}}{\mathrm{dt}} &= \frac{i}{C3} - \frac{V_{R_3C_3}}{R_3C_3} \end{aligned}\right\}, \tag{2}$$

where $(dV_{R_1C_1}/\mathrm{dt})$, $(dV_{R_2C_2}/\mathrm{dt})$, $(dV_{R_3C_3}/\mathrm{dt})$ presents the transient voltages.

The first, second, and third parallel RC networks' respective time constants are denoted by R_1C_1, R_2C_2, and R_3C_3. The discrete version of the equations created using ECM is represented as equation (3).

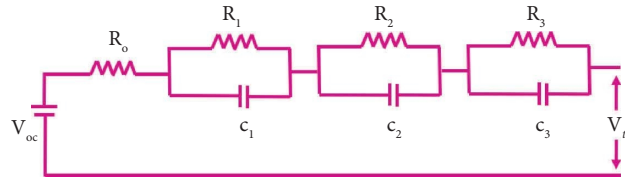

Figure 1: 3RC battery model.

$$\left.\begin{aligned} V_{1,j+1} &= V_{1,j}e^{(-\Delta T/\tau_1)} + \left[1 - e^{(-\Delta T/\tau_1)}\right]R_1 I_j \\ V_{2,j+1} &= V_{2,j}e^{(-\Delta T/\tau_2)} + \left[1 - e^{(-\Delta T/\tau_2)}\right]R_2 I_j \\ V_{3,j+1} &= V_{3,j}e^{(-\Delta T/\tau_3)} + \left[1 - e^{(-\Delta T/\tau_3)}\right]R_3 I_j \end{aligned}\right\}, \tag{3}$$

$$\left.\begin{aligned} &V_{t,j+1} = V_{oc,j+1} + R_0 I_{k+1}(t) + V_{1,j+1} + V_{2,j+1} + V_{3,j+1} \\ &j \in \{1, 2, \ldots N\} \end{aligned}\right\}, \tag{4}$$

where, τ_1, τ_2, and τ_3, indicate the time constant of the 3RC network.

The battery terminal voltages V_t, V_{oc}, and V_1, V_2, V_3 represent the open circuit voltage (OCV) and voltage drop across the 3RC branch's polarization resistance, respectively.

Equation (5) presents the formula to determine the battery's SOC.

$$\mathrm{SOC} = \mathrm{SOC}_o - \frac{\eta}{C}\int I(t)\mathrm{dt}, \tag{5}$$

C, capacity of the battery, SOC_o, initial SOC of the battery, and η is Coulombic efficiency. The current integration (Coulomb counting) method is used to determine the battery SOC. Since the self-discharge rate of Li-ion batteries is minimum, the coulomb efficiency value is close to 1.

$$\eta = \frac{\text{Capacity discharged}}{\text{Capacity charged}}. \tag{6}$$

According to equation (6), η lowers when more battery charge and discharge cycles are performed. Battery testing under charge and discharge circumstances yields a link between battery voltage and SOC.

The charging current is presented in the following equation:

$$I_{C,j}(t) = I_{B,j(t)} + I_{C,j(t)}, \tag{7}$$

I_C–Cell current, I_B–Balancing current.

The current and voltage of the pack is presented in equations:

$$I_{C,j}(t) = I_{C,j+1(t)}, j \in \{1, 2, \ldots . N-1\}, \tag{8}$$

$$V_o(t) = \sum_{j=1}^{N} V_j(t). \tag{9}$$

Battery system output is shown in the following equation:

$$\left.\begin{aligned} I_o(t) &= \sum_{j=1}^{N}\left(I_{\mathrm{Bo},j}(t) + I_{C,j}(t)\right) \\ P_o(t) &= V_o(t)I_o(t) \end{aligned}\right\}, \tag{10}$$

I_o is the output current, $I_{\mathrm{Bo},(t)}$ is the output current of the balancing circuit, and P_o is the power output of battery pack.

During the balancing process, the power balance equation for each cell is displayed in the following equation:

$$V_j(t)I_{B,j}(t) = V_o(t)I_{\mathrm{Bo},j}(t) + P_{\mathrm{lB},j}(t), \tag{11}$$

P_{lB} denotes the power loss across the balancing circuit.

$$\begin{aligned} I_B &= \frac{V_B}{R_B}, \\ P_{\mathrm{lB},j}(t) &= R_B I_{B,j}^2(t). \end{aligned} \tag{12}$$

The constraints of current in the battery balancing circuit are as follows:

$$I_{\mathrm{Bmin}} \le I_{B,j(t)} \le I_{\mathrm{Bmax}}, \tag{13}$$

I_{Bmax} and I_{Bmin} are the maximum and minimum balancing current limits for the circuit.

During balancing, the following constraints are imposed in order to achieve voltage and temperature equilibrium:

$$\left|V_j(t) - V_{\mathrm{avg}}(t)\right| \le \Delta_V, \tag{14}$$

where Δ_{V} is the highest typical cell-to-pack voltage disparity

$$\left|T_j(t) - T_{\mathrm{avg}}(t)\right| \le \Delta_T, \tag{15}$$

where Δ_T is the maximum temperature disparity between the average of each cell and the pack.

The change in battery temperature is calculated using the first-order differential equation, as given in the following equation:

$$T_B(t) = T_{\mathrm{int}} + \int_0^t \frac{\left[P_L - (T - T_a)/R_T\right]}{C_T}\,\mathrm{d}\tau, \tag{16}$$

where T_a represents the ambient temperature in degrees Celsius, T_B signifies the battery temperature in degrees Celsius, stands for the battery's initial temperature, which is set equal to the ambient temperature in degrees Celsius. C_T denotes thermal capacitance in Joules per degree Celsius, while R_T signifies thermal resistance in degrees Celsius per Watt. P_L represents the power loss across the battery's internal and polarization resistance. To calculate the power loss for the 3RC equivalent battery model, the following equation is used

$$P_L = I^2R_0 + I^2R_1 + I^2R_2 + I^2R_3. \tag{17}$$

The value of R_1, R_2, R_3, and R_0 are estimated at different SOC through EIS test.

3. Proposed System

In this work, a modular flyback converter is introduced for cell balancing. The primary aim of this approach is to address voltage imbalances within battery cells. This new architecture uses a transformer with numerous windings to separate the single input and multiple output terminals. Through a simple switch operation, the developed configuration ensures that the battery's voltage is kept stable when being charged or discharged. The usage of the conventional flyback converter [20] leads to excessive stress on the switch and the formation of ringing due to the primary electric field effect, potentially resulting in damage to the switch. Consequently, the switch experiences increased voltage stress caused by the input voltage. To address this issue, an individual clamp circuit is necessary to suppress voltage spikes and enable the flow of current through the magnetizing inductor when the switch is turned off. However, the presence of such a clamping circuit can lead to power dissipation through the resistance element, ultimately limiting the long-term power efficiency of the converter. To address the drawbacks of the conventional flyback converter a modular two-switch converter is designed. The developed configuration contains two switches ($Q1$ and $Q2$), alongside two diodes, $D1$ and $D2$, interconnected in a bridge configuration. When adapting a typical flyback converter circuit for cell balancing purposes, it transforms into a design in which four battery cells within a single transformer distribute the similar magnetic flux. In contrast to the conventional flyback converters, where the circuit necessitates a number of transformers equivalent to the number of cells, our proposed design allows for a reduction to just one transformer. This innovation harnesses shared magnetic flux to facilitate rapid voltage synchronization and straightforward voltage detection. Moreover, the use of modular flyback converters minimizes the impact of voltage spikes caused by leakage when compared to traditional single-switch converters, thereby enhancing overall battery performance. Figure 2 presents the basic configuration of the developed two-switch modular flyback converter. Figure 3 presents the modes of operation of the proposed converter, considering a single battery cell in the circuit.

In Figure 3(a), when both switches $Q1$ and $Q2$, each with a duty cycle ratio of D, are concurrently activated a connection is made between the input terminal and the transformer's primary winding. As a result, the diode in the secondary winding of the transformer receives a reverse voltage across its terminals. Consequently, during this period, the current within the secondary winding is obstructed, directing it to pass through the freewheeling diode, where it is transformed into reactive power. This results in a reduction in both power loss and system noise. The inductor current is given as

$$i_M = \frac{V_g}{L_M}\mathrm{DT}_s, \tag{18}$$

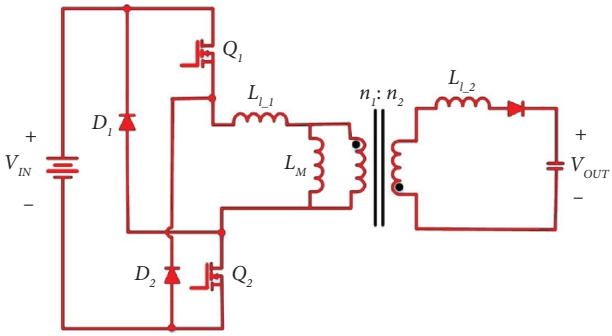

Figure 2: Proposed 2-switch flyback converter.

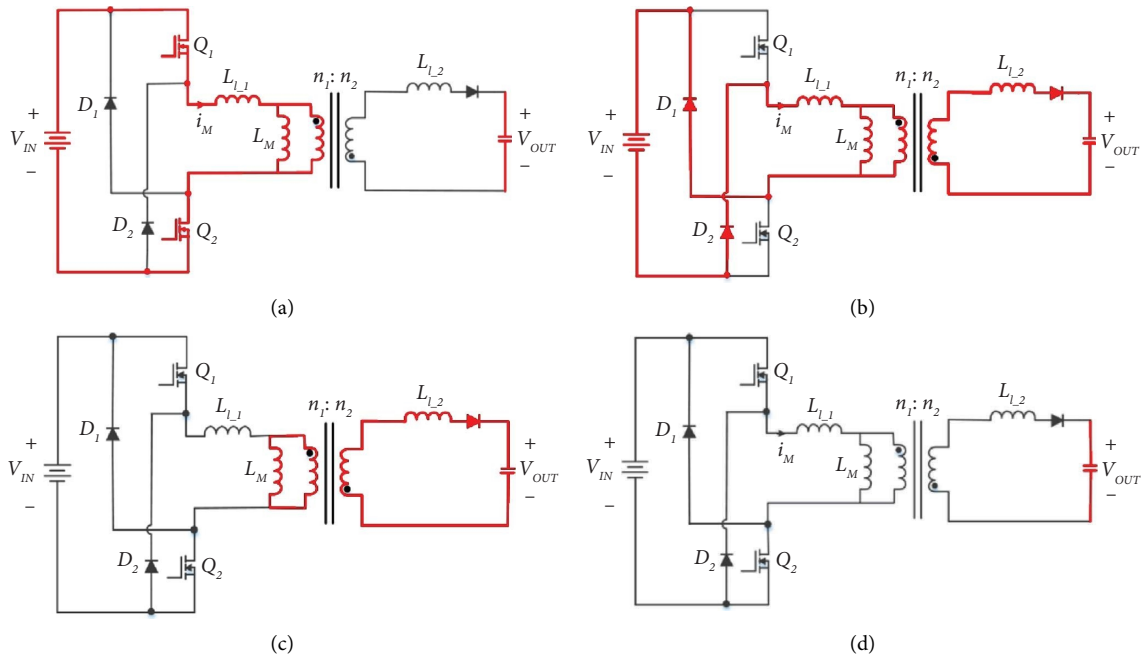

Figure 3: Modes of operation of the developed converter.

where V_g is the input voltage, and L_m is the magnetizing inductance.

Figure 3(b) illustrates the coordinated deactivation of switches $Q1$ and $Q2$. The current flowing through the magnetising inductor must continue in the same direction even after the switch is turned on and off; therefore, it is returned to the input terminal and reversed by the two freewheeling diodes. This leads to a linear decrease in the inductor current, denoted as i_M. Figure 4 portrays the equivalent circuit when both $Q1$ and $Q2$ are deactivated, assuming that the primary side current remains above zero

$$i_M = -\frac{n_1}{n_2}\frac{V_g}{L_M}(1-D)T_S. \tag{19}$$

Equation (20) displays the secondary winding current (i_{sec}) from the transformer.

$$i_{\text{sec}} = \frac{n_1/n_2 V_g - V_{\text{out}}}{L_{l_2}}. \tag{20}$$

Here, L_{l2} represents the secondary side transformer's leakage inductance, while V_{out} signifies the output voltage. The energy stemming from leakage is channeled back through the diode, transforming it into reactive power. This process results in a reduction in power loss and system noise. The determination of the operational mode at this stage relies on whether the step-down converter meets the conditions outlined in equation (21), thereby initiating the operation mode when the specified condition is met.

$$V_{\text{IN}} > \frac{n_1}{n_2} V_{\text{OUT}}. \tag{21}$$

Thus, when equation (21) is satisfied, the diodes play a role in enabling current flow through voltage inversion, thereby transferring energy from the primary side to the secondary side. In addition, the voltage equation governing the current on the secondary side remains in accordance with the following equation:

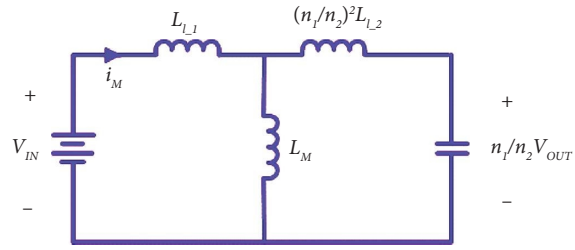

Figure 4: Equivalent circuit during the switch off condition.

$$\begin{bmatrix} V_{\mathrm{IN}} \\ V_{\mathrm{OUT}} \end{bmatrix} = \begin{bmatrix} -\left(L_{l_1} + L_M\right) & -L_M \\ -\dfrac{n_2}{n_1} L_M & -\left(\dfrac{n_1}{n_2} L_{l_1} + \dfrac{n_2}{n_1} L_M\right) \end{bmatrix} \begin{bmatrix} i_M \\ i_{\mathrm{sec}} \end{bmatrix}. \tag{22}$$

The primary side current (i_M) is given as follows:

$$\begin{aligned} i_M &= V_{\mathrm{OUT}} \\ &= \frac{1}{X}\left\{-\left(\frac{n_2}{n_1} L_{l\_2} + L_M\right) V_{\mathrm{IN}} + \frac{n_1}{n_2} L_M V_{\mathrm{OUT}}\right\}, \end{aligned} \tag{23}$$

Where,

$$\begin{aligned} X &= V_{\mathrm{OUT}} \\ &= \left(\frac{n_1}{n_2}\right)^2 L_{l\_2}\left(L_{l\_1} + L_M\right) + L_{l\_1} L_M. \end{aligned}$$

The operation of the circuit during this phase concludes when the primary current in the transformer reaches zero. Subsequently, as depicted in Figure 3(c), the inductor voltage also drops to zero. The amount of energy transferred within the magnetising inductor rapidly reduces when the current on the primary side of the transformer drops to zero. Ultimately, all currents within the modular flyback converter reach zero, as illustrated in Figure 3(d). Following this, switches $Q1$ and $Q2$ proceed to repeat the turn-on operation mode simultaneously.

4. Proposed Cell Balancing Method

Figures 5(a) and 5(b) depicts the operational mode of the proposed battery balancing method. As soon as $Q1$ and $Q2$ of the converter are turned off, energy is transferred through the transformer to the secondary cell stage, where it can be regulated to achieve a stable voltage. Thus, the power retained by the transformer is transferred to the cell stage via the transformer in conjunction with the electrical current passing via the diode during switch-on operation. Consequently, in situations where there exists a voltage imbalance among cells, the transformer's energy is equalized among them through their shared magnetic flux. Hence, as illustrated in Figure 6(a), the cell voltage undergoes a differential charging and distribution process, with the charging being differentially allocated based on the variance among the cell voltages. Conversely, if a specific cell voltage surpasses a predetermined threshold, it becomes imperative to halt the charging process automatically, thereby averting the risk of overcharging the battery cells. Consequently, as depicted in Figure 6(b), any excess energy exceeding the maximum charge voltage is transformed into reactive power and redirected back to the power supply source. This action effectively interrupts the distribution of voltage among the cells.

The transformer coil receives power from the primary side when the switch is turned on. This applied voltage's polarity is established by the direction of the current, while its amplitude is set by the duty cycle of the switch. In practise, cell balancing takes place when the converter switch is in its off position, as shown in Figure 7. Assuming a circuit is made up of two cells, m and l, at a given time, with different charging voltages, energy flows from the cell with the higher charging voltage to the cell with the lower charging voltage when the switch is off. Even as the number of cells increases, the charging principle can be used to calculate the magnitude and direction of energy transfer. Then, if cell' m' has a higher charging voltage (V_m) than cell 1 (V_l) cell' m' will charge faster.

$$i_{m \longrightarrow l} = \frac{V_m - V_l}{L_l}, \tag{24}$$

where L_l represents the leakage inductance, which serves as an impedance that restricts the flow of electricity. Figure 8 presents the three-winding transformer charging circuit of the proposed model. During this period, the cell's output voltage follows the equations (25)–(27) based on the specific magnetizing inductance conditions depicted in Figure 8.

$$v_p = L_p \frac{\mathrm{d}i_p}{\mathrm{dt}} + \mathrm{aM}_{P1} \frac{d}{\mathrm{dt}}\left(\frac{i_1}{a}\right) + \mathrm{bM}_{P2} \frac{d}{\mathrm{dt}}\left(\frac{i_2}{b}\right), \tag{25}$$

$$v_1 = \mathrm{aL}_1 \frac{\mathrm{d}}{\mathrm{dt}}\left(\frac{i_1}{a}\right) + M_{p1} \frac{\mathrm{d}i_p}{\mathrm{dt}} + \mathrm{bM}_{12} \frac{\mathrm{d}}{\mathrm{dt}}\left(\frac{i_2}{b}\right), \tag{26}$$

$$v_2 = \mathrm{Lp} \frac{\mathrm{d}i_p}{\mathrm{dt}} + \mathrm{aM}_{p1} \frac{\mathrm{d}}{\mathrm{dt}}\left(\frac{i_1}{a}\right) + \mathrm{bM}_{P2} \frac{\mathrm{d}}{\mathrm{dt}}\left(\frac{i_2}{b}\right)$$

Where,

$$a = \frac{M_{P2}}{M_{12}}, \tag{27}$$

$$b = \frac{M_{P1}}{M_{12}}.$$

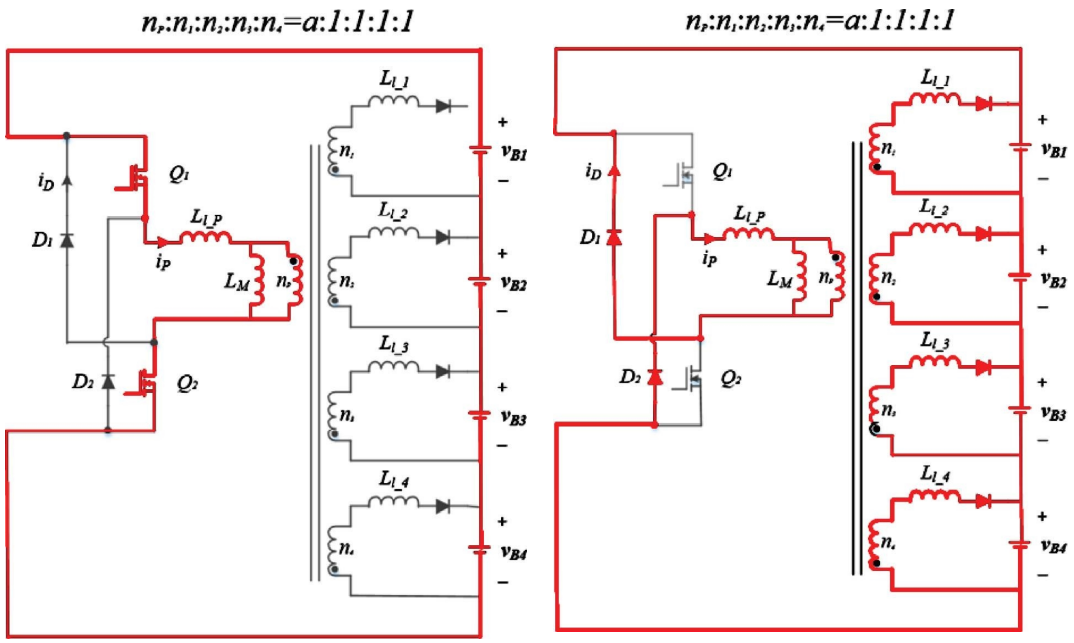

Figure 5: Proposed cell balancing method during (a) switch on and (b) off condition.

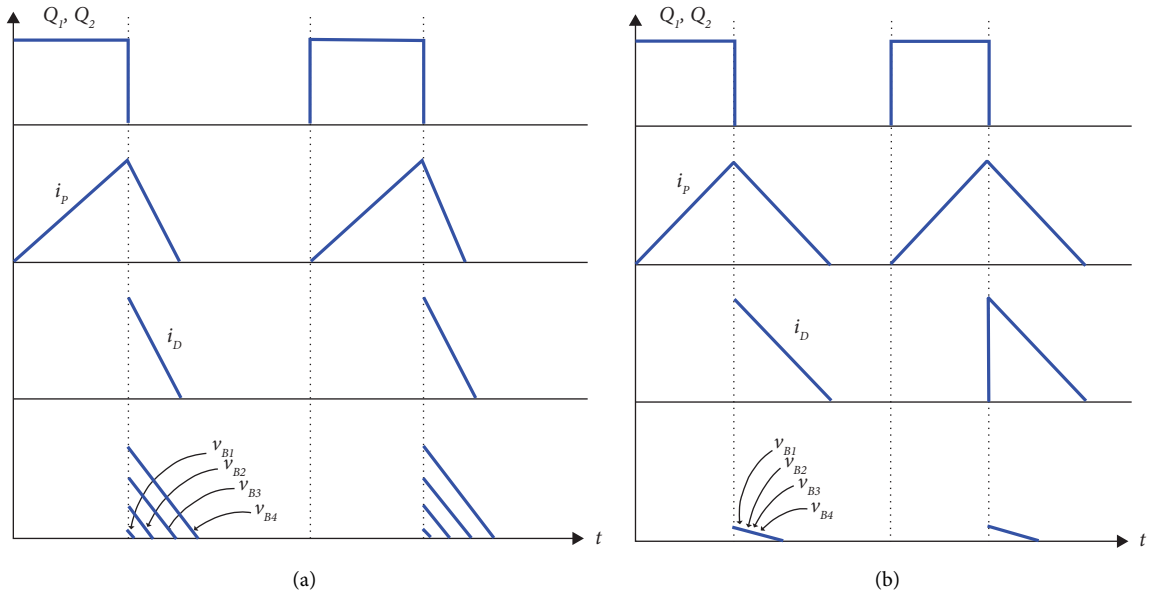

Figure 6: Graph (a) depicts the voltage balancing operation before the implementation of balancing control and (b) after balancing control has been applied.

This very principle remains applicable when the number of cells is expanded to n by augmenting the number of windings on the secondary side. Figure 9 presents the control of the proposed technique.

4.1. Comparison of the Proposed Method with Existing Methods. Table 1 provides a comparison of different balancing techniques with the proposed method, considering factors such as reliability, control strategy, balancing speed, and other relevant criteria. The choice of a cell balancing method is primarily guided by the control strategy and design principles that aim to minimize the use of hardware components. The control schemes, which encompass aspects like charge and discharge regulation, play a vital role in determining which method to employ. Despite the utilization of capacitor-based balancing systems during both charging and discharging phases, they exhibit an inherent efficiency of only 50%. Moreover, they are unsuitable for Li-ion battery chemistry, which demands a minimal degree of

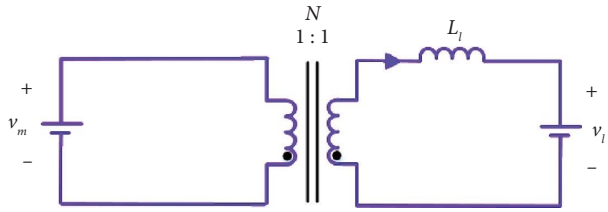

Figure 7: Voltage balancing between cells.

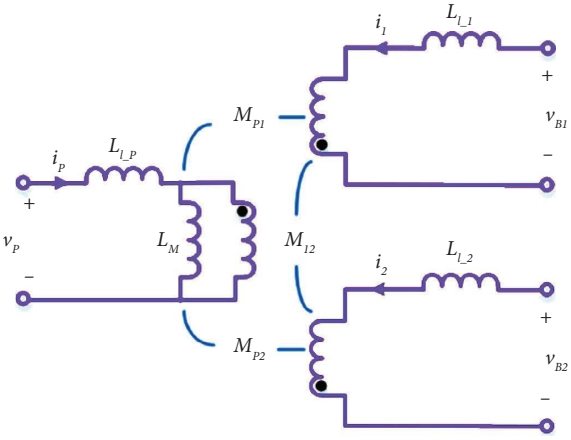

Figure 8: Multitransformer with cells.

voltage imbalance. In contrast, the transformer-based balancing system is more efficient than the inductor-based system and is characterized by greater complexity.

5. Results and Discussion

The simulation work is carried out for a 48V Li-ion battery pack with sixteen cells connected in series. The two switch flyback converter-based balancing architecture is implemented in Matlab/Simscape, specifically configured for charging conditions, to assess the performance of the framework. Parameter values for the model are stored in the lookup table. During the simulation, cells are charged in the CC-CV mode and the variation in voltage across the cells is determined by modifying the initial state of charge (SoC) of the battery pack. Each cell has a capacity of 3.3Ah, and an inductor value of 10μH has been selected. The simulation involves computing the open circuit voltage (OCV), terminal voltage, temperature, and SoC for each cell. At the outset, the voltage difference between cell1 and cell2 is intentionally maintained at a level exceeding 30mV. Once the cell voltages reach the designated charge threshold of 3.9V during a charging rate of 0.5C, the process of cell balancing is triggered. The first phase, Stage 1, commences by activating switch Q1 and Q2 as soon as cell 1's voltage surpasses that of cell 2. Subsequently, switch S1 is kept in the ON state, leading to the charging of inductor 1, and it remains ON until the voltage differential between the cells falls below 30mV. Energy stored in inductor 1 is then transferred to cell 2 after approximately 5,800 seconds via the body diode of switch Q2. The graph in Figure 10 displays minimal fluctuations in cell voltage due to the low balancing threshold voltage applied. Figure 11 presents the SoC of the cell1 and 2. As illustrated in Figure 11, the entire charging process consumes approximately two hours to reach completion, with cell balancing requiring approximately 50 minutes. Charging takes place in an environment maintained at 20°C. During the charging process, cell temperatures gradually rise, peaking at 24.75°C as depicted in Figure 12. Despite voltage fluctuations during charging, the current remains constant. As each cell reaches its maximum voltage, it switches to the constant voltage mode, as illustrated in Figure 13. In this mode, voltage is held steady while current gradually decreases to the lowest permissible level based on power rating.

Passive and the proposed balancing system simulation results reveal that passive balancing takes longer time due to greater voltage discrepancies among cells, as evidenced in Figures 14 and 15. The proposed balancing method, as shown in Figures 16 and 17, effectively addresses the limitations of passive balancing. The rise in temperature near the battery pack is attributed to heat generated by the balancing system, which accelerates battery aging mechanisms and reduces overall battery life. To analyse the temperature characteristics of the balancing system, two key parameters, maximum temperature ($T_{\max}$) and temperature distribution (ΔT), among the cells are assessed. The active system exhibits a lower maximum temperature (24°C) compared to the passive system (27°C), and ΔT does not exceed 4°C during the charging process, as depicted in Figures 18 and 19. The simulation results provide a wealth of important metrics, such as power dissipation, equilibrium duration, energy dissipation, energy effectiveness, and the overall expense of the equilibrium system. Tables 2 and 3 exhibit the results of simulations for both passive and active scenarios in a standard 48 V electric bicycle (E-bike) system. When passive balancing is employed, it becomes apparent that a substantial energy loss occurs only when there is a high degree of imbalance. In contrast, the proposed topology consistently demonstrates low energy loss, regardless of the extent of imbalance or the quantity of imbalanced cells within the battery pack. In low-power E-bikes, where the voltage requirements are relatively modest, the occurrence of cell imbalances is notably reduced. In the case of a fourteen-cell series-connected battery pack, the passive balancer required 48 minutes to bring the cell voltages below the balancing threshold (30 mV), as illustrated in Figure 14. Passive balancing exhibits minimal power dissipation, as indicated in Table 2, making it the practical choice for these scenarios.

Proposed balancing, on the other hand, is not a viable option due to its circuit complexity and high cost. Therefore, passive balancing finds its applicability in low-power E-bikes. In situations where a significant voltage deviation exists (e.g., due to aged cells) and a greater number of imbalanced cells (resulting from multiple charge-discharge cycles), the passive balancer took 215 minutes to achieve balance but incurred a power loss of 4.55W, as detailed in Table 3. Given the substantial losses observed (as indicated in Table 3), opting for the proposed balancer becomes a more compelling choice. The proposed balancer, as shown

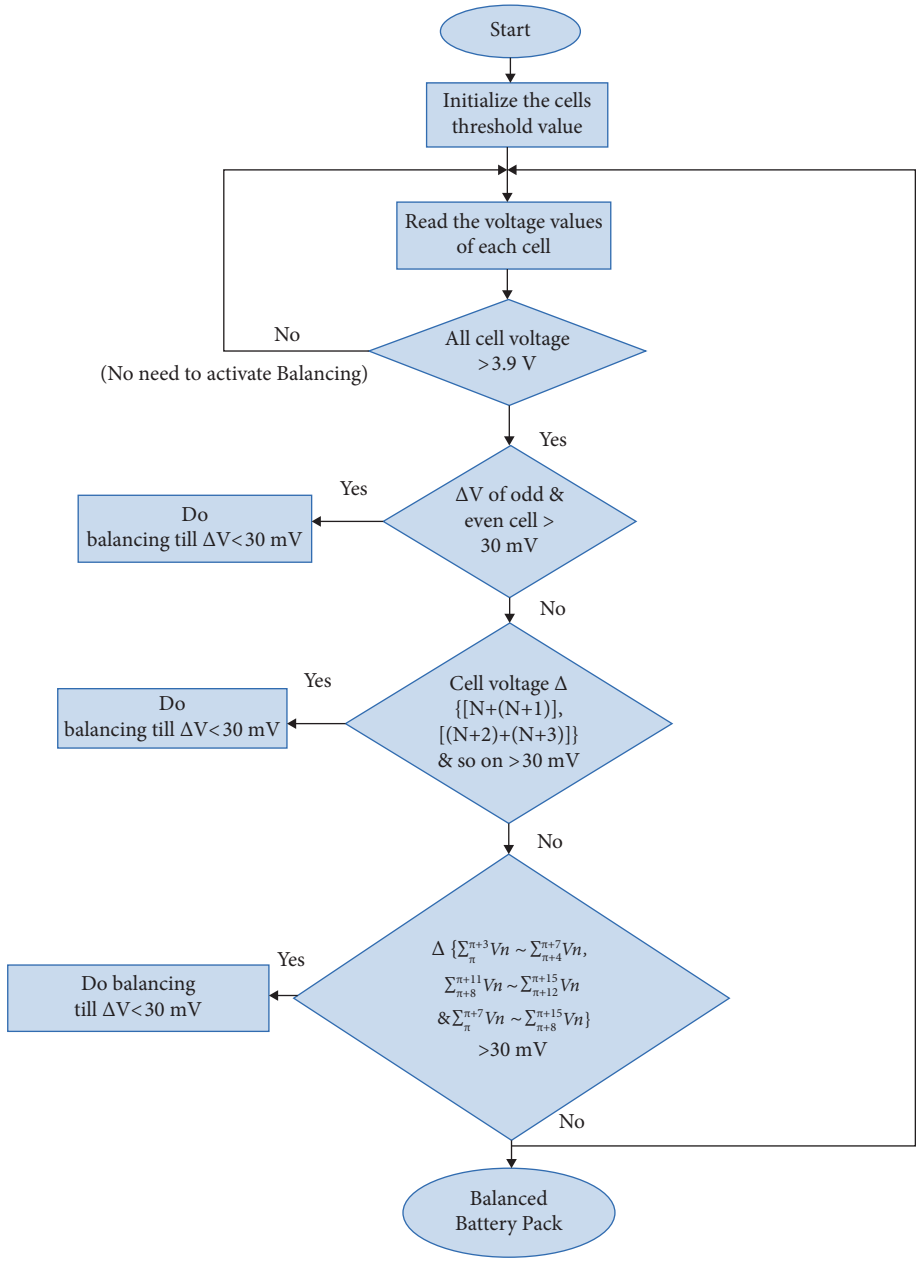

Figure 9: Control of the proposed method.

in Table 3, managed to balance the cells within a range of 30 mV–200 mV in a significantly shorter time frame, taking between 15 and 42 minutes. A comparative analysis of cell balancing system characteristics among various electric vehicle (EV) variants is presented in Table 4. It is evident that although passive balancing reduces power loss, it does not yield significant cost savings from energy loss mitigation. Moreover, the passive balancing system's propensity for generating hot spots within the battery pack can have adverse effects on the battery's remaining useful life (RUL) and state of health (SOH) due to the high-energy losses it incurs. Figure 20 presents the comparison of the passive and proposed method with various balancing characteristics.

5.1. Integration of Electric Cars into Microgrid Using a 24-Hour Simulation of the Vehicle-to-Grid System. The integration of electric cars as energy storage systems into the microgrid is carried out using MATLAB. The design of a vehicle-to-grid (V2G) system is presented in Figure 21. This work mainly focuses on the impact of energy storage during off-grid and on-grid operations by analysing the active power graph. Electric vehicles that connect to the grid have only local information, and the voltage profiles of other nodes are unknown. The total number of electric cars in this simulation design is 100, and all of the electric cars combine to form one energy storage aggregator with a power output of 4 MW, as shown in the model specification of the energy storage aggregator in Table 5.

Table 1: Comparative study of proposed balancing scheme with the existing balancing methods.

Ref	Balancingspeed	Reliability	Controlstrategy	Cost	Size	%η
[21]	£	Щ	Ъ	Й	Б	£
[22]	ļ	Щ	Ш	Щ	Ш	£
[23]	Щ	Щ	Щ	Й	Ш	Й
[24]	£	£	Ъ	Й	Ш	Щ
[16]	£	£	Ш	Й	Č	Щ
[25]	Щ	Щ	Ъ	Щ	Ш	Щ
[26]	£	£	Ш	Щ	Ш	Щ
[27]	Й	Щ	Ъ	£	Č	Й
[28]	Щ	Щ	Ъ	Щ	Ш	Щ
[29]	Й	Й	Ъ	Щ	Ш	Й
[30]	£	ļ	Ъ	£	Ш	Щ
[31]	£	ļ	Ъ	£	Ш	£
Proposed	£	ļ	Ш	£	Ш	Й

£-low, ļ-very low, Ъ-hard, Й-high, Щ-medium, Ш-moderate, Č-compact, Б-bulk.

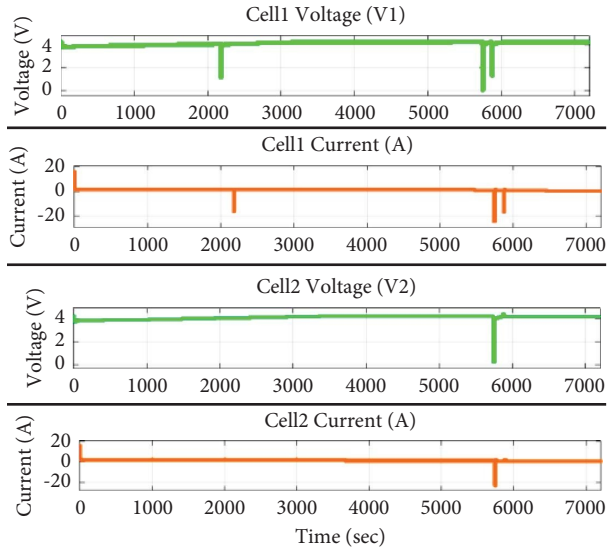

Figure 10: Voltage and current of cells 1 and 2.

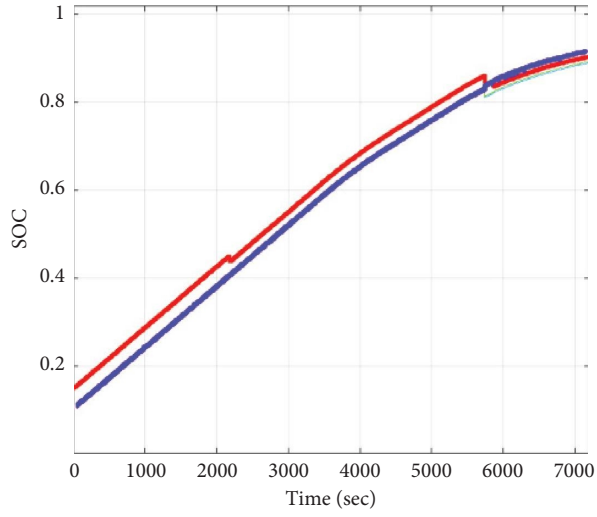

Figure 11: SoC of cells 1 and 2.

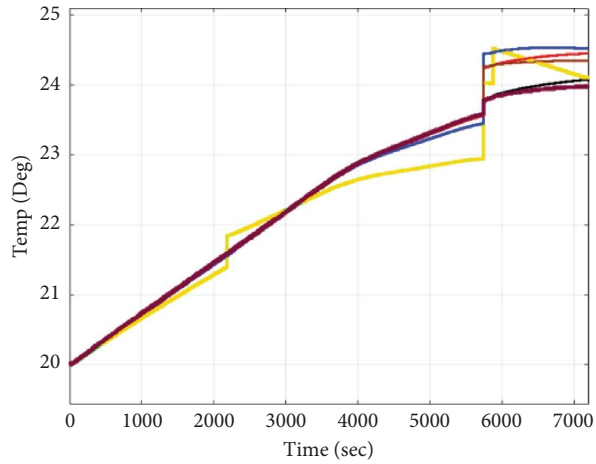

Figure 12: Battery temperature.

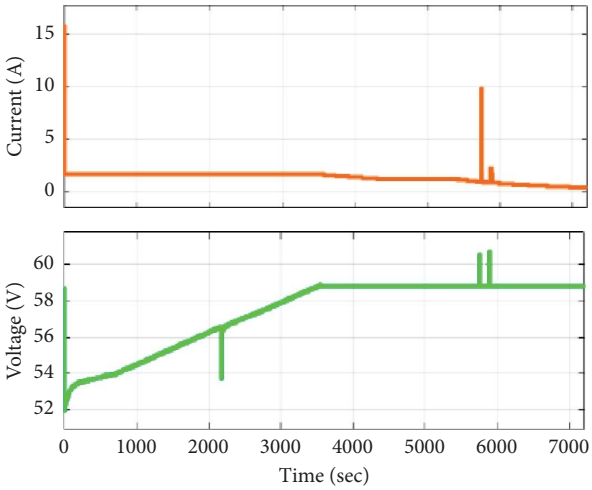

Figure 13: Charging voltage and current.

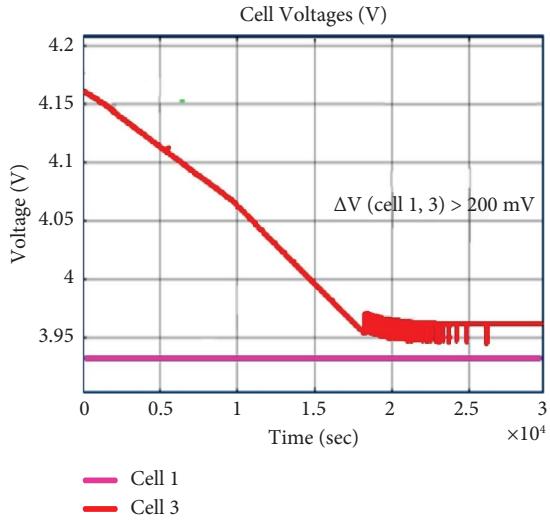

Figure 15: Passive balancing (idle).

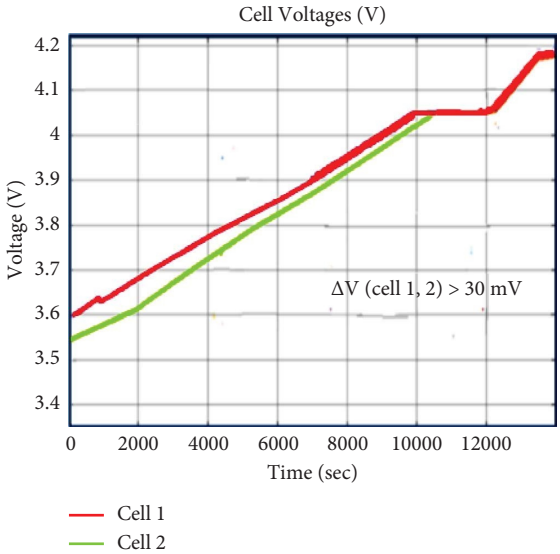

Figure 14: Passive balancing (charging).

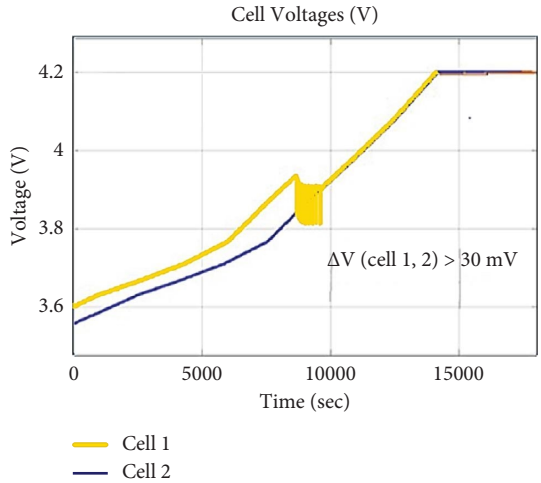

Figure 16: Proposed balancing method (charging).

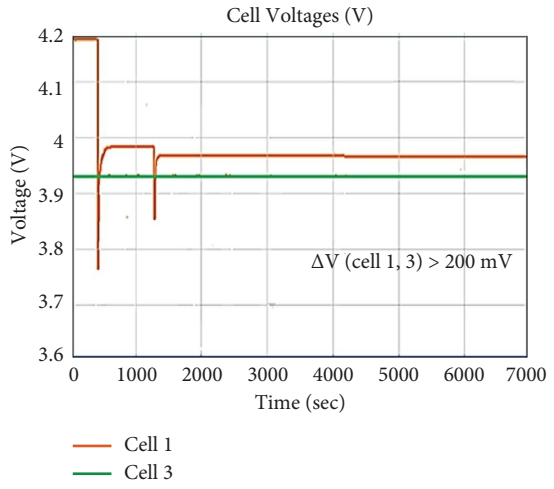

Figure 17: Proposed balancing method (idle).

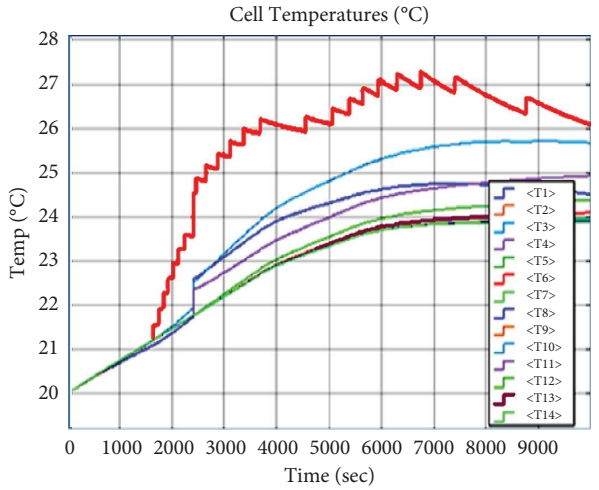

Figure 18: Temperature rise (passive).

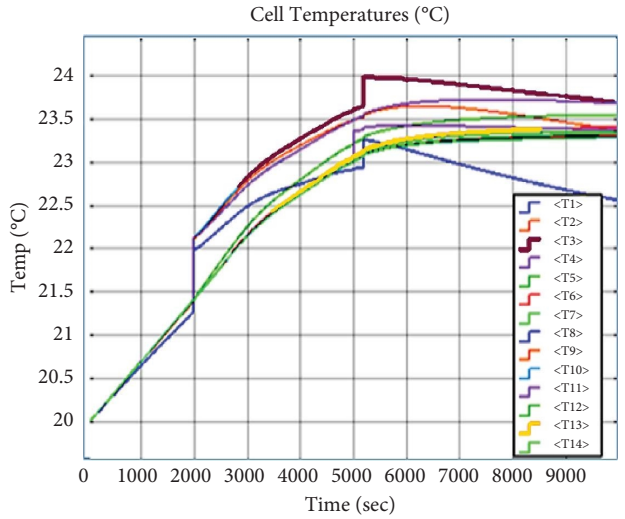

Figure 19: Temperature rise (proposed).

Table 2: Calculation of the energy efficiency and cost associated with the passive system.

ΔV (mV)	Cells (#)	P_{loss} (W)	BT (min)	E_{loss} (Wh)	ŋ (%)	Cost ($)
30	1	0.37	48	0.25	98.11	0.07
	13	4.45	48	3.14	96.52	0.35
200	1	0.25	215	1.15	99.02	0.11
	13	4.05	215	14.50	93.33	1.89

Table 3: Calculation of the energy efficiency and cost associated with the developed system.

ΔV (mV)	Cells (#)	P_{loss} (W)	BT (min)	E_{loss} (Wh)	ŋ (%)	Cost ($)
30	1	0.04	13	0.12	99.9	0.002
	13	0.89	17	0.33	99.7	0.039
200	1	0.57	29	0.21	99.56	0.028
	13	1.02	44	0.71	99.21	0.101

Table 4: Comparison of cell balancing system characteristics.

Parameters	E – Bike		E – Car		E – Truck	
	Passive	Proposed	Passive	Proposed	Passive	Proposed
Cells in series	14	14	96	96	250	250
ΔV (mV)	30	30	30	30	30	30
P_{loss} (W)	4.55	1.05	38	9.5	99.6	24.9
BT (Min)	48	20	48	20	48	20
E_{loss} (Wh)	3.64	0.35	30.4	3.2	80	8.3
ŋ (%)	97.8	99.7	97	99	96.7	98.5
E_{loss} cost ($)	0.49	0.05	4.05	0.4	10.7	1.11

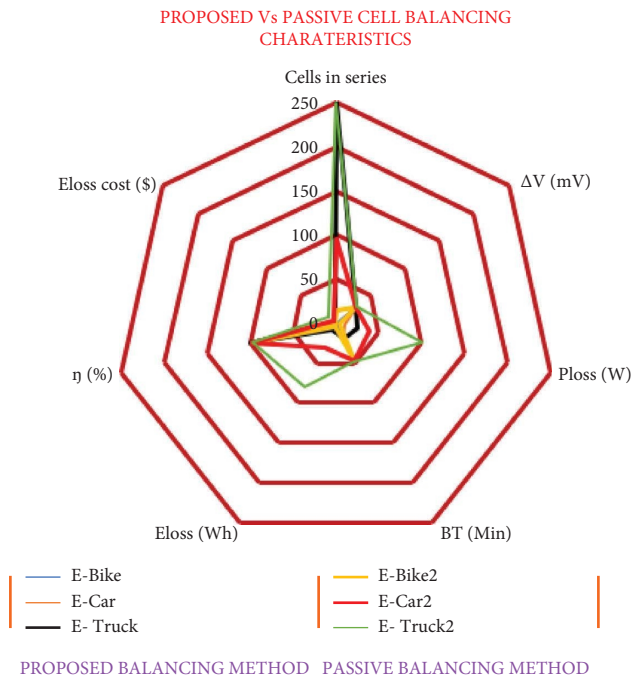

Figure 20: Comparison of the passive and proposed method with various balancing characteristics.

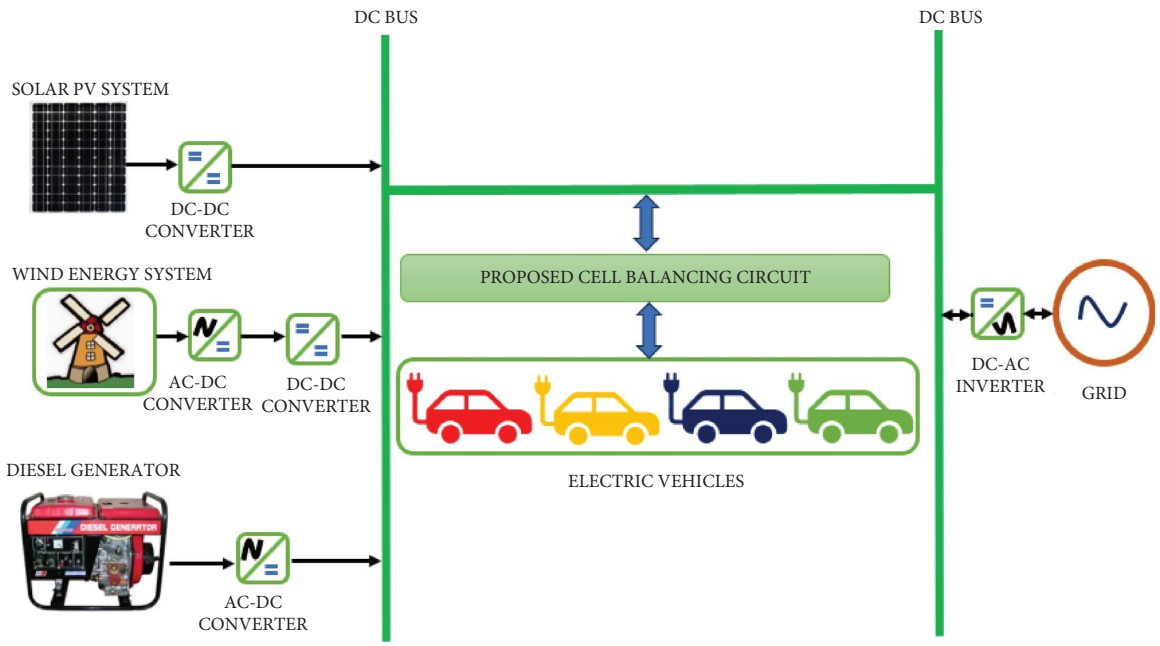

Figure 21: Design of the vehicle-to-grid system.

Table 5: Specification of an energy storage aggregator for a vehicle-to-grid (V2G) system.

Rated power for each electric vehicle		40 kW
Rated capacity		85 kWh
System efficiency		90%
Regular gain	K_p	2
	K_i	4000
Number of cars	Profile 1	35
Number of cars	Profile 2	25
Number of cars	Profile 3	10
Number of cars	Profile 4	20
Number of cars	Profile 5	10

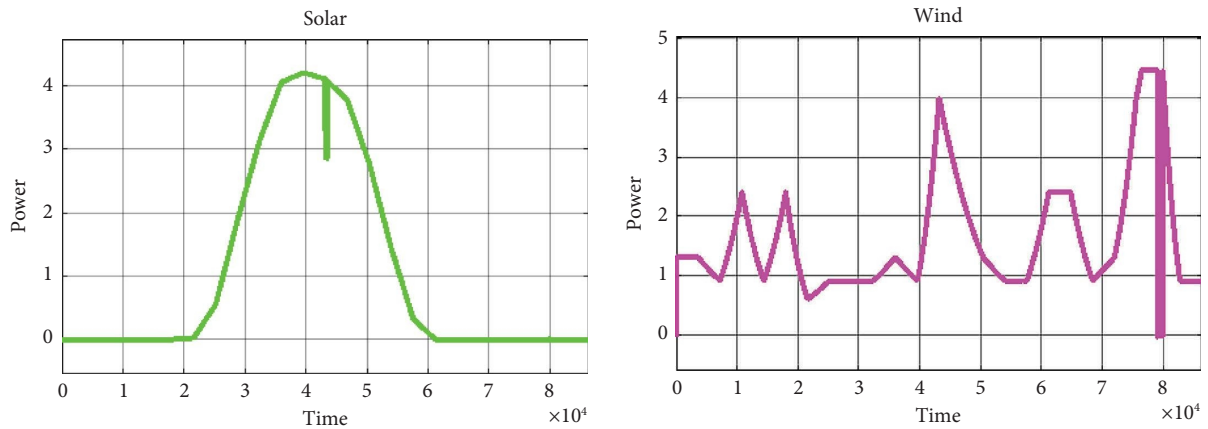

Figure 22: Continued.

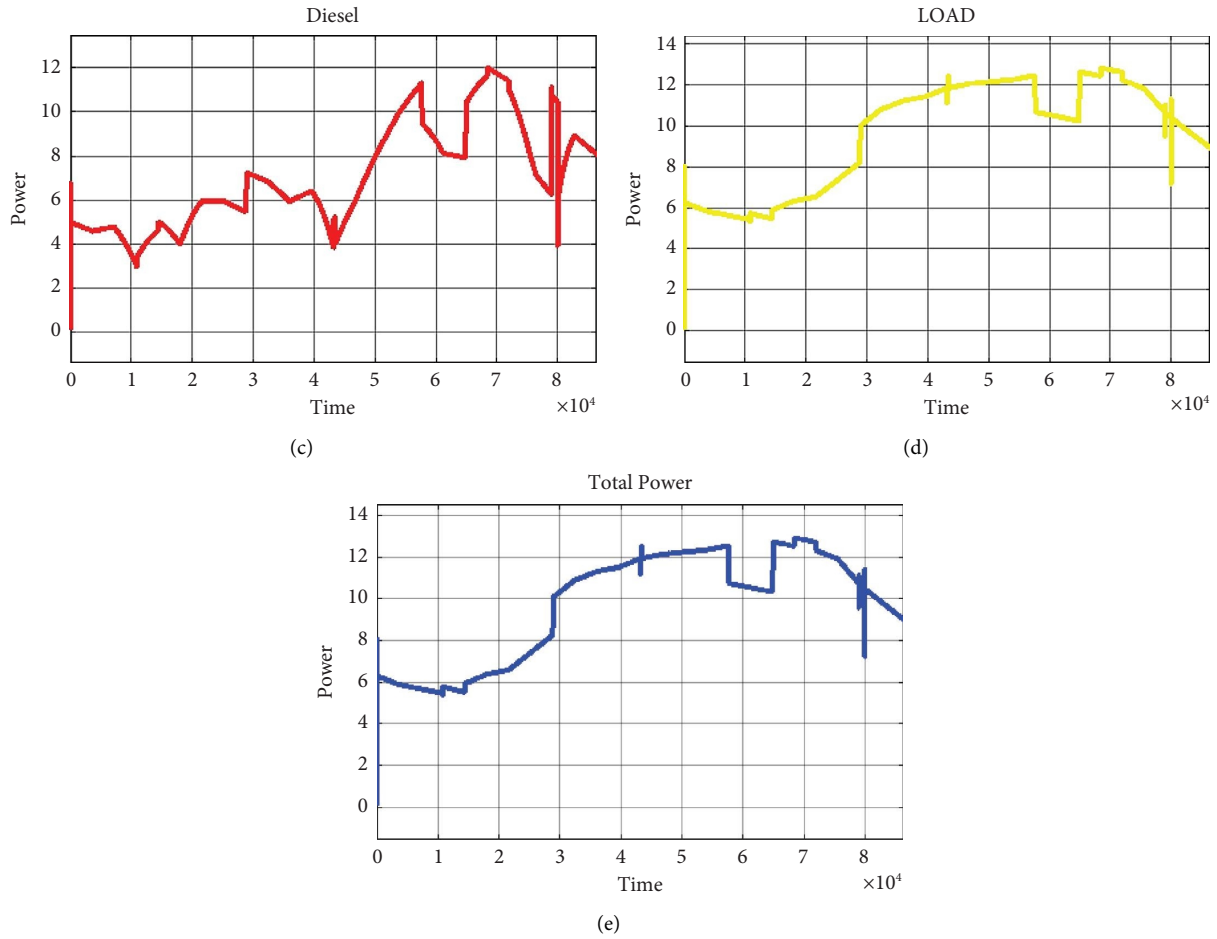

Figure 22: Simulation output when energy storage (electric vehicles) is connected to microgrid.

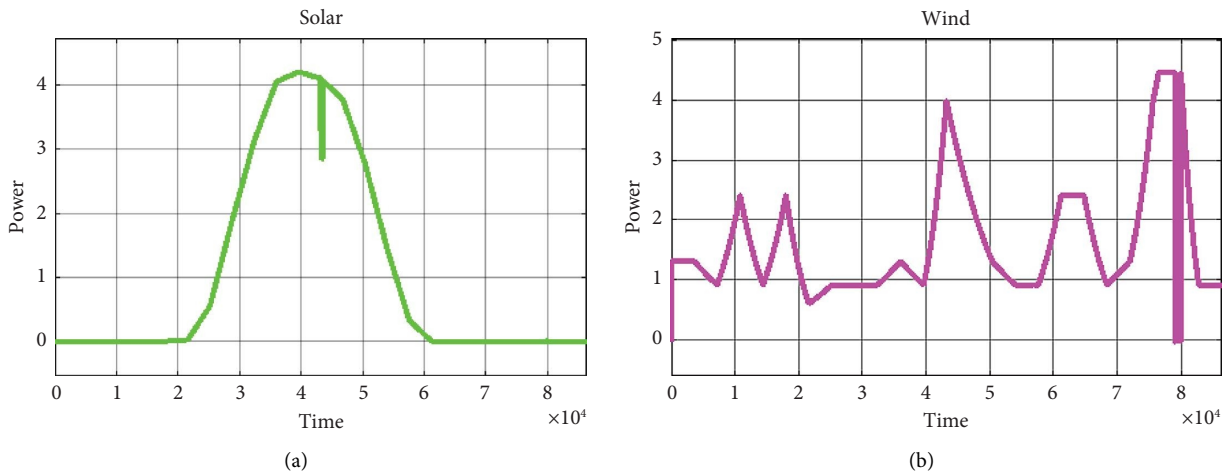

Figure 23: Continued.

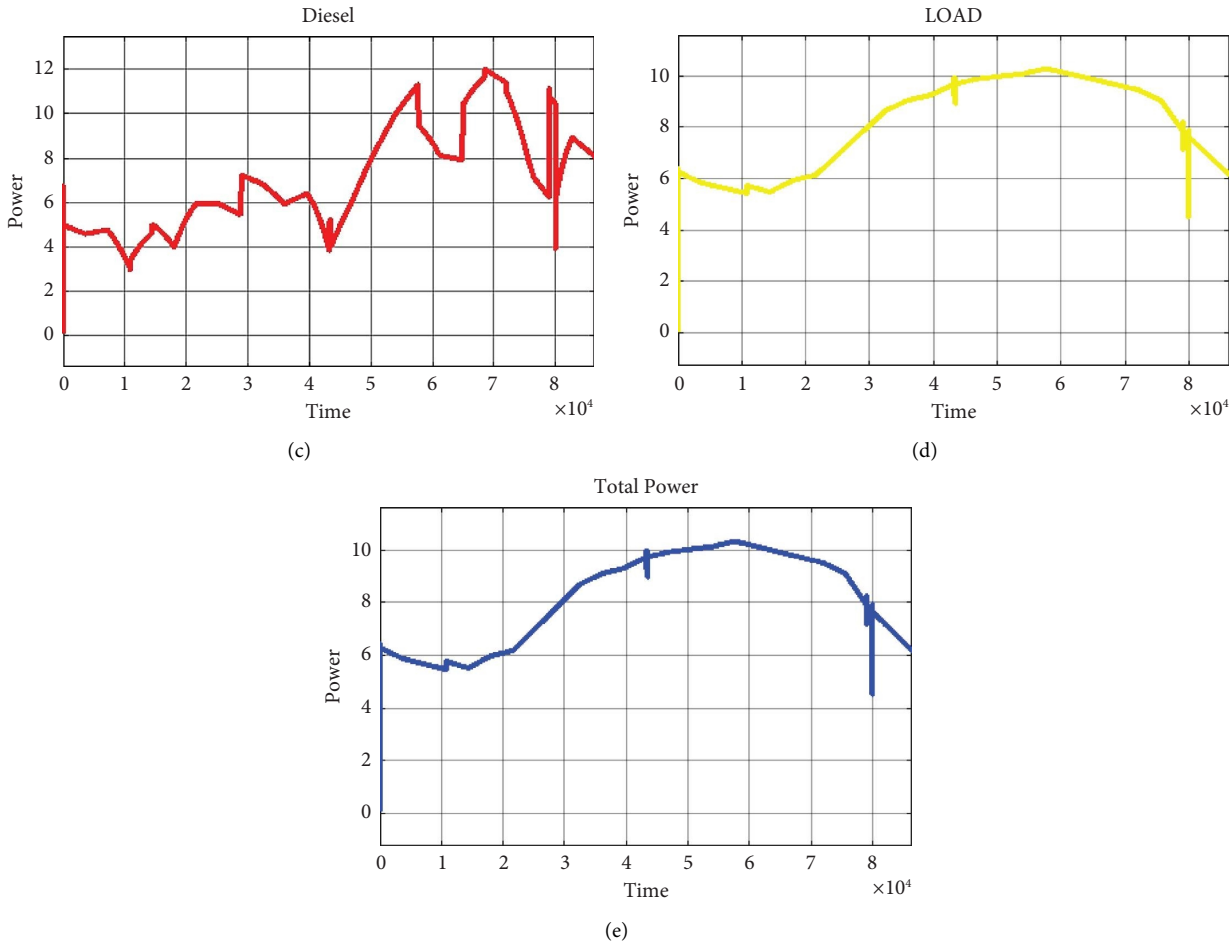

Figure 23: Simulation output without energy storage (electric vehicles).

Two different scenarios are simulated using a vehicle-to-grid system, including one case in which the energy storage aggregator that combines all-electric vehicles is connected to the microgrid, known as on-grid, and another one case in which the energy storage aggregator is disconnected from the microgrid, known as off-grid. The impact of electric vehicles connected to the power grid is studied in the first phase simulation, and the results of the active power in first phase is shown in Figure 22. The second phase of simulation investigates the impact of electric vehicles disconnected from the network, and the results of the active power graph is shown in Figure 23. From the Figures 22 and 23 the following observations have been done: vehicle-to-grid (V2G) technology allows power to flow from electric vehicles to the grid, transforming them into not only a distributed load but also a distributed storage and generation system. This is shown by the active power graph as energy storage transitions from off-grid to on-grid operation. The transition of energy storage from off-grid to on-grid demonstrates that connected electric vehicles add to the pre-existing peak active power of off-grid operation and provide an even higher peak active power during on-grid operations. This proves that energy storage plays an important role in increasing total energy generation during on-grid operation. Electric vehicle energy storage integration can be used as spare energy storage for grid support during peak load periods and can reduce the use of battery packs connected to a PV system during periods of high electrical demand, which can benefit the microgrid.

6. Conclusion

This paper introduces a two-switch flyback converter for balancing the cells of a lithium-ion battery. The developed battery balancing method has been implemented, and its performance has been compared with the passive balancing method. The modular design of the converter allows faster cell balancing. It can handle multiple cells simultaneously, which speeds up the balancing process, especially in large battery packs. The two-switch topology can help reduce stress on the switches, potentially extending their lifespan. An advanced control algorithm is implemented for precise and adaptive cell balancing, optimizing the battery's overall performance. Furthermore, the developed method is used in EVs which are combined as one energy storage aggregator and integrated into microgrids. The impact of connecting and disconnecting the energy storage from the microgrid shows that the overall active power of the microgrid

increased in pre-existing peak value from off-grid operation into on-grid operation. This emphasizes the fact that energy storage by using electric vehicles causes power flows in two directions, which not only distributes load but also distributed storage and generation to the microgrid.

Data Availability

The data used to support the findings of this study are available from the corresponding author upon request.

Conflicts of Interest

The authors declare that they have no conflicts of interest.

Acknowledgments

The research was funded by Centre for Research of Innovation & Sustainable Development (CRISD) of University of Technology Sarawak, Malaysia, University Research Grant, Grant/Award Number: UTS/3/2022/06.

References

[1] B. S. Hartono, Budiyanto, and R. Setiabudy, "Review of microgrid technology," in *Proceedings of the 2013 International Conference on Quality in Research, QiR 2013-In Conjunction with ICCS 2013*, pp. 127–132, Yogyakarta, Indonesia, June 2013.

[2] F. Jabari, S. Nojavan, B. Mohammadi Ivatloo, and M. B. B. Sharifian, "Optimal short-term scheduling of a novel tri-generation system in the presence of demand response programs and battery storage system," *Energy Conversion and Management*, vol. 122, pp. 95–108, 2016.

[3] A. Mohammad, R. Zamora, and T. T. Lie, *Integration of Electric Vehicles in the Distribution Network: A Review of PV Based Electric*, Springer, Berlin, Germany, 2020.

[4] Z. B. Omariba, L. Zhang, and D. Sun, "Review of battery cell balancing methodologies for optimizing battery pack performance in electric vehicles," *IEEE Access*, vol. 7, pp. 129335–129352, 2019.

[5] F. Justin, G Peter, A. A. Stonier, and V. Ganji, "Power quality improvement for vehicle-to-grid and grid-to-vehicle technology in a microgrid," *International Transactions on Electrical Energy Systems*, vol. 2022, Article ID 2409188, p. 17, 2022.

[6] F. Jabari, H. Arasteh, A. Sheikhi-Fini, and B. Mohammadi-Ivatloo, "Optimization of a tidal-battery-diesel driven energy-efficient standalone microgrid considering the load-curve flattening program," *International Transactions on Electrical Energy Systems*, vol. 31, no. 9, Article ID e12993, 2021.

[7] F. Jabari, H. Jabari, B. Mohammadi-ivatloo, and J. Ghafouri, "Optimal short-term coordination of water-heat-power nexus incorporating plug-in electric vehicles and real-time demand response programs," *Energy*, vol. 174, pp. 708–723, 2019.

[8] F. Jabari, M. Shamizadeh, and B. Mohammadi-ivatloo, "Dynamic economic generation dispatch of thermal units incorporating aggregated plug-in electric vehicles," in *Proceedings of the 3rd International conference of Iran Energy Association (IEA)*, Tehran, Iran, October 2017.

[9] D. Thiruvonasundari and K. Deepa, "Optimized passive cell balancing for fast charging in electric vehicle," *IETE Journal of Research*, vol. 69, no. 4, pp. 2089–2097, 2023.

[10] S. A. Hussien, A. BaQais, and M. Al-Gabalawy, "Battery management system enhancement for lithium-ions battery cells using switched shunt resistor approach based on finite state machine control algorithm," *Frontiers in Energy Research*, vol. 11, no. 2023, Article ID 1191579, 2023.

[11] S. Kumar, S. K. Rao, A. R. Singh, and R. Naidoo, "Switched-resistor passive balancing of Li-ion battery pack and estimation of power limits for battery management system," *International Journal of Energy Research*, vol. 2023, Article ID 5547603, 21 pages, 2023.

[12] Y. Li, P. Yin, and J. Chen, "Active equalization of lithium-ion battery based on reconfigurable topology," *Applied Sciences*, vol. 13, no. 2, p. 1154, 2023.

[13] K. Manjunath, R. Kalpana, B. Singh, and R. Kiran, "A two-stage module based cell-to-cell active balancing circuit for series connected lithium-ion battery packs," *IEEE Transactions on Energy Conversion*, pp. 1–15, 2023.

[14] T.-E. Fan, S.-M. Liu, H. Yang, P.-H. Li, and B. Qu, "A fast active balancing strategy based on model predictive control for lithium-ion battery packs," *Energy*, vol. 279, Article ID 128028, 2023.

[15] X. Lai, B. Li, X. Tang, Y. Zhou, Y. Zheng, and F. Gao, "A quantitative method for early-stage detection of the internal-short-circuit in Lithium-ion battery pack under float-charging conditions," *Journal of Power Sources*, vol. 573, no. 2023, Article ID 233109, 2023.

[16] Y. Ye, J. Wang, and X. Wang, "A multi-winding transformer-based active cell equalizer with self-driven switches for series-connected lithium-ion batteries and super-capacitors," *Journal of Energy Storage*, vol. 70, no. 2023, Article ID 107971, 2023.

[17] R. Aghapour, M. Zeraati, F. Jabari, M. Sheibani, and H. Arasteh, "Cybersecurity and data privacy issues of electric vehicles smart charging in smart microgrids," in *Electric Vehicle Integration via Smart Charging: Technology, Standards, Implementation, and Applications*, pp. 85–110, Springer International Publishing, Cham, Switzerland, 2022.

[18] D. Shylla, R. Swarnkar, R. Harikrishnan, and M. A. Sawal Hamid, "Active cell balancing during charging and discharging of lithium-ion batteries in MATLAB/simulink," in *Proceedings of the 2023 Second International Conference on Electronics and Renewable Systems (ICEARS)*, pp. 201–208, IEEE, Tuticorin, India, March 2023.

[19] Y.. Xia, "Comparison and analysis of SOC estimation based on first-order and second-order Thevenin battery models based on EKF," *Academic Journal of Science and Technology*, vol. 6, no. 3, pp. 10–18, 2023.

[20] C. Kumar, "Bi-directional DC-DC flyback converter using zero voltage switching for hybrid electric vehicle application," in *Proceedings of the 2023 9th International Conference on Advanced Computing and Communication Systems (ICACCS)*, vol. 1, pp. 894–899, IEEE, Coimbatore, India, March 2023.

[21] X. Zhang, G. Zhou, and S. Liu, "Switched-capacitor equalizers using hybrid balancing paths for series-connected energy storage cells," *Journal of Energy Storage*, vol. 63, Article ID 107112, 2023.

[22] S. Karmakar, K. B. Tushar, and A. Kumar Bohre, "Review on cell balancing technologies of battery management systems in electric vehicles," in *Proceedings of the 2023 IEEE IAS Global Conference on Renewable Energy and Hydrogen Technologies (GlobConHT)*, pp. 1–5, IEEE, Male, Maldives, March 2023.

[23] X. Guo, Q. Wu, C. Xing, W. Qian, and Y. Zhao, "An active equalization method for series-parallel battery pack based on

an inductor," *Journal of Energy Storage*, vol. 64, no. 2023, Article ID 107157, 2023.

[24] N. Vikhorev, A. Kurkin, D. Aleshin, D. Ulyanov, M. Konstantinov, and A. Shalukho, "Battery dynamic balancing method based on calculation of cell voltage reference value," *Energies*, vol. 16, no. 9, p. 3733, 2023.

[25] M. Abareshi, M. Hamzeh, S. Farhangi, and S. M. M. Alavi, "Robust control of a forward-converter active battery cell balancing," *IET Power Electronics*, vol. 16, no. 8, pp. 1271–1280, 2023.

[26] C. Shidling, "Active cell balancing using A flyback converter simulation in Matlab simulink," 2020, https://cselectricalandelectronics.com/active-cell-balancing-using-a-flyback-converter-simulation-in-matlab-simulink/.

[27] N. Nordin, S. Nuratma, F. R. Muhammad Izuan, L. H. Fang, M. Z. Aihsan, and M. S. Saidon, "Review article: voltage balancing method for battery and supercapacitor as energy storage," *Journal of Advanced Research in Applied Sciences and Engineering Technology*, vol. 29, no. 3, pp. 235–250, 2023.

[28] Y.-S. Lee, C.-Y. Duh, G.-T. Chen, and S.-C. Yang, "Battery equalization using bi-directional Cuk converter in DCVM operation," in *Proceedings of the 2005 IEEE 36th Power Electronics Specialists Conference*, pp. 765–771, IEEE, Recife, Brazil, June 2005.

[29] A. Samanta and S. Chowdhuri, "Active cell balancing of lithium-ion battery pack using dual DC-DC converter and auxiliary lead-acid battery," *Journal of Energy Storage*, vol. 33, no. 2021, Article ID 102109, 2021.

[30] Y. Shang, C. Zhang, N. Cui, and J. M. Guerrero, "A cell-to-cell battery equalizer with zero-current switching and zero-voltage gap based on quasi-resonant LC converter and boost converter," *IEEE Transactions on Power Electronics*, vol. 30, no. 7, pp. 3731–3747, 2015.

[31] M. Kumar, V. K. Yadav, K. Mathuriya, and A. K. Verma, "A brief review on cell balancing for Li-ion battery pack (BMS)," in *Proceedings of the 2022 IEEE 10th Power India International Conference (PIICON)*, pp. 1–6, IEEE, Delhi, India, November 2022.